Mathematical Biosciences 257 (2014) 60–68

Contents lists available at ScienceDirect

Mathematical Biosciences

journal homepage: www.elsevier.com/locate/mbs

Transdermal transport pathway creation: Electroporation pulse order

Sid Becker [a,*], Barbara Zorec [b], Damijan Miklavčič [b], Nataša Pavšelj [b]

[a] University of Canterbury, Christchurch, New Zealand
[b] University of Ljubljana, Ljubljana, Slovenia

ARTICLE INFO

Article history:
Available online 10 July 2014

Keywords:
Skin electroporation
Thermodynamic
Stratum corneum
Numerical
Experimental

ABSTRACT

In this study we consider the physics underlying electroporation which is administered to skin in order to radically increase transdermal drug delivery. The method involves the application of intense electric fields to alter the structure of the impermeable outer layer, the stratum corneum. A generally held view in the field of skin electroporation is that the skin's drop in resistance (to transport) is proportional to the total power of the pulses (which may be inferred by the number of pulses administered). Contrary to this belief, experiments conducted in this study show that the application of high voltage pulses prior to the application of low voltage pulses result in lower transport than when low voltage pulses alone are applied (when less total pulse power is administered). In order to reconcile these unexpected experimental results, a computational model is used to conduct an analysis which shows that the high density distribution of very small aqueous pathways through the stratum corneum associated with high voltage pulses is detrimental to the evolution of larger pathways that are associated with low voltage pulses.

1. Introduction

Advances in pharmacy and biotechnology have yielded a number of drugs that have shown promise in achieving good therapeutic results. Current trends show increased interest in the field of dermal and transdermal drug delivery. However, the skin's outer barrier, the *stratum corneum* (SC), offers the greatest resistance to molecular transport. Transdermal drug delivery methods focus on methods of overcoming this barrier function of the SC [1,2]. This study considers the physics underlying electroporation which involves the application of intense electric fields to alter the barrier's microstructure. By exposing the skin to electroporation pulses, the SC experiences a structural alteration that results in orders of magnitude increase in molecular diffusivity, electrophoretic mobility, and electrical conductivity.

The increase in the skin's permeability to transdermal delivery after skin electroporation depends on the electric pulse characteristics (i.e. amplitude, duration, number and frequency). The expert opinions in the field are in general agreement that there are different responses according to two primary pulsing regimes: (i) that short duration-high intensity pulses result in an altered SC that is perforated with nano- to micrometer-sized aqueous "pores", and (ii) that long duration medium intensity pulses result in regions of increased permeability within the SC that are relatively large (up to hundreds of μm) but that occur at a much lower density (number of pathways per SC surface area) than the high voltage (HV)-created pathways [3–15].

The structural alterations associated with the short pulse regime are probably related to the initiation of nanoscale aqueous defects into the SC's lipid microstructure. Experimental observations show that when the voltage drop across the SC exceeds some critical value (above ~30 V) the skin experiences a sudden increase in permeability to molecular transport of up to four orders of magnitude within less than ~10 μs [8]. The mechanism associated with alteration of the SC lipid structure during the HV pulses can be attributed to the interaction between the water dipole and the electric field. In molecular dynamics (MD) studies of single bilayer electroporation it has been shown that it is the polarity of water (and not the charge of the lipid head groups) that is responsible for the initiation of pores within the lipid structure [16,17]. The nanoscale aqueous pathways that are initiated within the first few μs of exposure to the electric field are a result of the interaction between the applied electric field and individual water molecules that are located at the surface of the SC and within any lipid structure defects throughout the interior of the SC.

The response of the skin in the long pulse regime occurs at much longer timescales (up to hundreds of ms) and is associated with the development of large regions of altered SC (up to hundreds of μm). The large region of affected SC that results from this expansion is termed the "Local Transport Region" (LTR) because within this region the permeability to molecular transport is

* Corresponding author. Tel.: +64 3 364 2987x7231.
E-mail address: sid.becker@canterbury.ac.nz (S. Becker).

http://dx.doi.org/10.1016/j.mbs.2014.07.001
0025-5564/

several orders of magnitude higher than in the surrounding unaltered SC. These LTRs are formed within the sites of the so-called *stratum corneum* "defects" [4] which have a higher electrical conductivity than the surrounding SC so that under the application of the low voltage (LV) electric pulses, the current density within these defects is high. The development of the LTR is believed to be associated with resistive (Joule) heating which has been documented under certain experimental pulse conditions to cause localized temperature rises of over 60 °C [3,6,9,10,18–21].

Based on published empirical data, the conclusion might be drawn that the skin's increase in permeability to molecular transport is proportional to the number of pulses administered (regardless of pulse type HV or LV). For example in the review by Denet [8] a compilation of data on the transdermal delivery of Fentanyl (net charge +1, MW 337 Da) shows that the total delivery increases with the number of pulses as well as with the pulse amplitude. This trend has been repeatedly shown in many experimental studies over the years. The conclusion from this can be drawn that more electric pulses will result in more transport regardless of the pulse characteristics. While this may be true for the transdermal delivery of solute of low molecular weight, an incorrect conclusion may be drawn that the increase in permeability (for all solutes) is proportional to the total power of the pulses. The authors of the present work believe that this is a false interpretation of the data and that one must consider the physics associated with pulse type in addition to the total power of the applied pulses.

Recently we have conducted experimental electroporation tests that provide results that are not really in agreement with the general view held by the field [22]. In fact the authors have shown that under certain pulsing protocols, the total transport of solute is *decreased* with the addition of more pulses. It is the motivation of this study to provide a preliminary investigation in which we consider the underlying physics responsible for LTR evolution and attempt to reconcile our experimental findings indicating that when long moderate voltage pulses are preceded by short intense pulses, the total transport is less compared to the case when long moderate pulses are administered alone.

2. Experimental results

The computational model presented is used to try to explain the empirical observations of *in vitro* experiments on dermatomed porcine skin. The experimental component of this paper follows an identical methodology to that reported previously [22]. The transport of calcein (molecular charge: 4−) was studied in vertical glass Franz diffusion cells (skin surface available for diffusion: 0.785 cm^2), thermo regulated at 37 °C by water circulation. A unipolar square wave pulse generator Cliniporator (Igea, Italy) was used for pulse delivery. The pulses were delivered into the donor and the receiver compartment through 1 mm diameter platinum wire electrodes placed 0.2 cm away from the skin in donor compartment and 0.5 cm in the receiver compartment. Different combinations of high voltage (HV) and low voltage (LV) pulses were used in the study (see Fig. 1). The parameters of the HV pulses were: 500 V, 500 μs duration, 500 μs spacing between pulses (when applicable). Further the parameters of LV pulses were: 45 V, 250 ms duration, 100 ms pulse spacing (when applicable). Further, only about 30% of the voltage delivered with the pulse generator into the donor and the receiver solution was established across dermatomed skin. This skin voltage – U_{skin} – was measured during pulse delivery, as well as the electric current through the sample.

We monitored concentration of calcein in the receiver solution every hour for five hours of passive diffusion after pulse delivery. The concentration of calcein was measured with spectrofluorometer (Jasco, FP-6300). One way ANOVA was performed on all results as a statistical test (SigmaStat 3.1, Systat, USA). A 0.05 level of probability was taken as a level of significance. The results are expressed as the mean ± standard error of the mean (normality test passed in all instances). For further details about the experimental part of the study, we refer the reader to [22].

In Fig. 1 we present the experimentally obtained total concentration of calcein in the receiver solution, measured every hour for five hours of passive diffusion after pulse delivery. As expected, the control without an applied pulse to interfere with the barrier function of the SC results in negligible calcein concentration at five hours of passive diffusion after pulse delivery. On the other hand, only negligible rise in calcein delivery can be observed after 3 × HV pulse protocol, implying that the cell-size pathways through the SC created by short (500 μs duration) high voltage (HV) pulses are too small for significant enhancement of subsequent transdermal transport. A statistically significant improvement in the passive delivery of calcein following pulse delivery is accomplished only after longer LV pulses are added to the protocol. This is consistent with a very large increase in SC permeability that is anticipated in the creation of large LTRs which are associated with long LV pulses.

It is important to note that the system response to transport is very strongly tied to the exact conditions under which the experiments are conducted. Furthermore, the results depicted in Fig. 1 are specific to the delivery of calcein and should not be interpreted

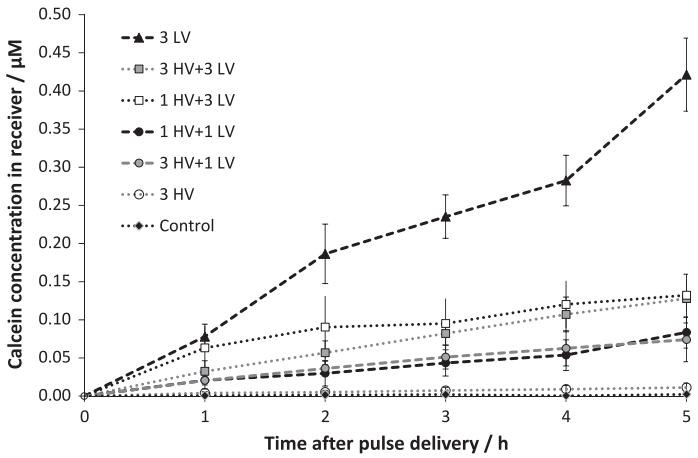

Fig. 1. Comparison of different combinations of short (500 μs) HV (high voltage) and longer (250 ms) LV (low voltage) pulses and their effect on calcein concentration in the receiver solution for 5 h of passive diffusion after pulse delivery. Pulses were delivered at time zero.

as a general statement of the increases in permeability to electroporation pulse. For example solute of much lower molecular weight is anticipated to be able to penetrate even the very small paths that are initiated by the HV pulses.

This result (that HV pulses result in lower transport than LV pulses) is anticipated based on our understanding of the pulsing responses. Note that the HV pulses result in a high density number of cell-sized pathways within the SC, while LV pulses are expected to result in much larger regions of increased permeability. However, what we did not expect in the experiment was the skin's response to a combination of HV and LV pulses.

We found that HV pulses have a negative effect on calcein delivery compared to LV pulses alone (see Fig. 1). In fact, passive transport of calcein through the skin after pulse delivery increases with increasing number of LV and decreases with increased number of HV pulses. This was contrary to our expectations which lie on the assumption that regardless of the pulse type (HV or LV) more pulses will result in an overall lower resistance to transport. We, in fact, anticipated that the physics would result in a two step process in which: (1) the short, HV pulses result in the creation of small cell-level permeation pathways through the stratum corneum and then (2) that by following the HV pulses with the LV pulses, these pathways would evolve into the much larger LTRs. The experimental results, however, seem to indicate that the anticipated physics are not correct. This in fact is the motivation of the theoretical component of this study: to try to reconcile the experimental results with the generally accepted belief that more pulses equal greater drops in the resistance to transport. For more in-depth discussion on the experimental results we refer the reader to Ref. [22].

In the subsequent sections a detailed description of a numerical model is made. This model is used to capture the response of the skin to the LV pulses. The model is then used to arrive at a mechanistic based explanation of the experimental findings which seem to run contrary to our initial expectations drawn from the general view held in the field.

3. Theoretical model

The theoretical model presented in this paper will link the structural alterations of the SC and electrical conductivity to the transport of solute. The thermodynamic model used here describes the thermo-electrical behavior in a small region of the skin sample. This is depicted in Fig. 2. This region is centered directly around an evolving LTR so that unless otherwise stated, the outer radius of the computational domain (R_O) is 250 μm. It should be noted that the lateral surface area modeled here is 1/400th of that of the actual experiment whose outer radius was 5 mm. While the results here apply only to this small region of the skin, the idea is that there is a distribution of LTRs within the actual skin sample each of whose behavior is reflected by the results of the theoretical model.

3.1. Thermal–electrical model

To capture the sudden temperature rise associated with resistive heating of the skin during an electroporation pulse, the heat equation is used to describe the transient distribution of thermal energy within each layer of the system:

$$\rho_i c_i \frac{\partial T}{\partial t} = \nabla \cdot (k_i \nabla T) + Q_J(z, r, t) \tag{1}$$

where ρ is the density, c is the specific heat, k is the thermal conductivity, and T is the temperature. The subscript i refers to any one of the elements or skin layers: donor solution, electrode, SC, epidermis or dermis. Because the study only models the experimental *in vitro* setup with dermatomed skin (thickness approx. 350 μm), blood perfusion and metabolic heat generation are orders of magnitude smaller and can safely be neglected from Eq. (1). The resistive heating, Q_J occurs only during the applied electric pulse, and is defined as:

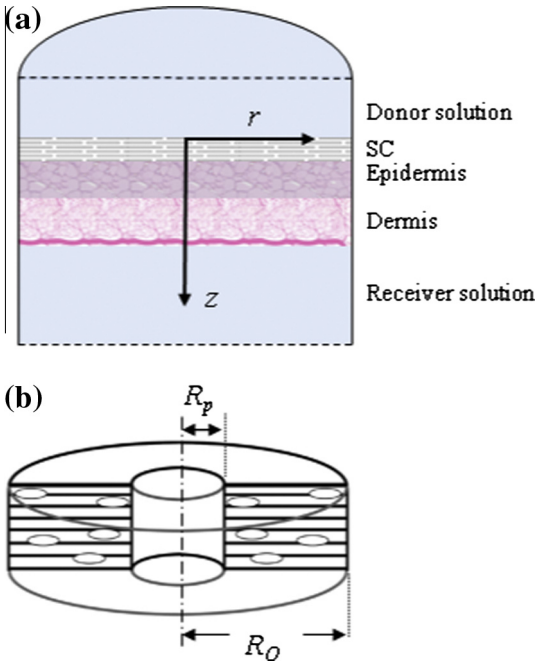

Fig. 2. The cylindrical representation of the domain modeled. (a) The composite representation of the skin sample set between the donor and the receiver solutions; (b) a closeup of the pre-existing SC defect of radius R_P set within the radial domain of outer radius R_O. In the theoretical representation the region about a single LTR is modeled. Thus depending on pore density, the domain of the theoretical model represents between 0.04 and 0.001 of the entire lateral surface area of the experimental skin sample.

$$Q_J = \sigma_i |\nabla V|^2 \tag{2}$$

where σ is the electrical conductivity and V is the electric potential, which is solved from the Laplace equation:

$$\nabla \cdot (\sigma_i \nabla V) = 0 \tag{3}$$

Because the steady-state DC electric field is established at a time scale much shorter than that which is associated with thermal conduction and electrically assisted diffusion of calcein, the transient effects can safely be neglected. In fact the capacitive charging times are so short that they can be safely neglected even for the shortest HV pulses used in this study (500 μs duration). In order for a localized high current density to evolve, the SC electrical conductivity should be modeled to have some initial lateral variation. This can be represented by a small region with a much higher relative local electrical conductivity, and in the experiment, this would correspond to a skin defect or appendage such as a sweat gland or hair follicle. The pre-existing pathways modeled in the computations of this study have an outer radius (depending on the particular case) of between 2.5 μm and 10 μm. The region within this defect is assigned the same electrical properties as the donor solution layer (roughly the same as those of the solution). The system response is strongly tied to the local electrical conductivity. This is evident from Eqs. (2) and (3). An over estimation of the pore electrical conductivity will likely result in greater initial resistive heating, and the results of this study should be considered with this in mind. This is probably an overestimation of the

conductivity within the pore although it is clear that the electrical conductivity of the defect region should be much higher than in the surrounding SC.

3.2. Transport model

Transport model in this study is derived from the modified Nernst–Planck equation which describes the transport of a charged solute in the presence of an electric field:

$$\frac{\partial C}{\partial t} = \nabla \cdot [(D_i \nabla C) + (m_i C \nabla V)] \tag{4}$$

where m is the effective electrophoretic mobility, D is the diffusion coefficient, and C is the dimensionless solute concentration which has been normalized by the relation: $C = C^*/C_0$ where C^* is the local solute concentration and C_0 is the initial homogenous solute concentration within the donor solution. Even long electroporation pulse times are usually only tens to hundreds of ms long so that the influences of electro-osmosis are negligible compared to the electrophoretic contributions [8,23,24] and have been neglected from Eq. (4). During the application of the pulse, the contribution of diffusion is also much smaller than that electrophoresis and has been theoretically shown to play no role in the transport of large charged solute at small time scales [25]. However at times between pulses, or after the application of a series of pulses (e.g. for 5 h after pulse delivery), the diffusion is the only transport mechanism. The subscript "i" refers to one of the layers: solution, SC, epidermis, or dermis. The evolving LTR, from a mass transport perspective represents a region whose transport coefficients are drastically increased. The next challenge is to try to map the increase in transport coefficient to the evolution of the LTR.

3.3. Degree of LTR formation

To link the thermal model to the alteration of the SC lipids that exist within the SC's LTR, we have previously developed a thermodynamic approach that reflects the experimental observation of SC lipid thermal studies [25–27]. A parameter is introduced that is called the lipid melt fraction and represents the ratio of heat added to the SC lipids (above phase transition temperatures) to the total heat required to complete a full transition of the SC lipid structure:

$$\varphi = (H(T) - c_{SC}T)/\Delta H \tag{5}$$

where ΔH is the latent heat associated with the phase transition, and $H(T)$ is total enthalpy defined as:

$$H = \int_{T_1}^{T_2} c_{SC,APP}(T)dT \tag{6}$$

where $c_{SC,APP}$ is the SC apparent specific heat. The transition takes place over the temperature range $[T_1, T_2]$. The parametric values used to describe Eqs. (5) and (6) are referenced from experimental data provided in [28] and are: $T_1 = 65$ °C, $T_2 = 75$ °C, $\Delta H = 5300$ J/kg K. To simplify the description considerably, a rectangular shaped specific heat vs. temperature curve is used [25] so that Eq. (6) may be represented as:

$$\varphi = \begin{cases} 0: & T \leqslant T_1 \\ \frac{T-T_1}{T_2-T_1}: & T_1 \leqslant T \leqslant T_2 \\ 1: & T_2 \leqslant T \end{cases} \tag{7}$$

The melt fraction is a description of the state of the lipids within the developing LTR. Uninfluenced lipid structures will have a melt fraction of $\varphi = 0$ while fully altered lipids will have a melt fraction of $\varphi = 1$. Within the SC, the transport coefficients of Eq. (4) (D_{SC} and m_{SC}) may be related to the melt fraction using a linear function so that:

$$\begin{aligned} m_{SC} &= m_{SC\text{-}U} + \varphi(m_{SC\text{-}M} - m_{SC\text{-}U}) \\ D_{SC} &= D_{SC\text{-}U} + \varphi(D_{SC\text{-}M} - D_{SC\text{-}U}) \end{aligned} \tag{8}$$

The estimation of the transport coefficients within the SC's unaltered lipid filled spaces, $m_{SC\text{-}U}$, $D_{SC\text{-}U}$ and within the "melted" lipid filled spaces, $m_{SC\text{-}M}$, $D_{SC\text{-}M}$, must be to some extent empirical. Values of all transport coefficients used in this study are provided in Table 1 and will be discussed in the following section. Similarly, the increase in SC electrical conductivity of Eqs. (2) and (3) is:

$$\sigma_{SC} = \sigma_{SC,U} + \varphi(\sigma_{SC,M} - \sigma_{SC,U}) \tag{9}$$

where $\sigma_{SC\text{-}U}$ is the SC electrical conductivity associated with the unaltered lipid structure ($\varphi = 0$), and $\sigma_{SC\text{-}M}$ is the electrical conductivity associated with the SC after full lipid melting ($\varphi = 1$). The conductivity values listed in Table 1 have been chosen to represent the two order of magnitude increase in electrical conductivity with lipid restructuring as suggested by Ref. [13].

3.4. Parametric considerations

Geometric parameters used in this model were taken as representative of porcine ear skin from Ref. [29]. Electrical conductivity values of the epidermis and dermis were representative of values published in [30]. The electrical properties of the solution are similar to that of water. The *SC* is assumed to be transverse by a pre-existing appendageal pore and this is represented in the radial center by a cylindrical region of whose thermophysical properties are equal to the donor/receiver solutions. Thermodynamic and geometric values shown in Table 1 are taken from previous studies that model the layered nature of the skin [25–27,31].

The transport coefficients of calcein are conservative and have been chosen based on interpretation of previous work. The diffusion coefficient of the calcein in solution is chosen based on the estimated diffusion coefficient calcein in water of 6×10^{-10} m^2/s [32] and of calcein in pH 8 boric acid-tris buffer $\sim 2.4 \times 10^{-10}$ m^2/s [33].

The electrophoretic mobility of calcein in solution is chosen to reflect experimentally determined values of calcein in a concentration of 0.1 mM in a solution of ~6–7 pH [34].

Exact diffusivity and mobility values of calcein in the epidermis and viable dermis are likely to fluctuate greatly depending on the condition of the skin sample. We have considered the results of studies studying the relative decrease in electrophoretic mobility of fluorescent dextran in water compared to the mobility in brain tissue to find a reduction of around 60% [35] or even up to 85% [36]. Clearly these studies do not correlate precisely to the relation of transport coefficient in the deeper regions of the skin. However, we use these as a guide to analyze the transport behavior of calcein within the dermis and lower epidermis extra-cellular matrix.

The unmodified (unaltered by electroporation) SC is modeled as nearly impermeable to calcein in this study and this is reflected in the extremely low transport coefficient values for regions of the SC that are uninfluenced by lipid thermal behavior (or the non-thermal effects of the HV pulses). We have chosen five orders of magnitude to show increases in transport coefficients associated with the fully altered LTR. The diffusion coefficient and electrophoretic mobility are strongly influenced by porosity and tortuosity, and it is well established that the lipid filled spaces of the SC are highly tortuous and not very porous [28]. The diffusion coefficients associated with the fully altered SC lipids within the LTR have been chosen to reflect this. The relative effect of porosity related permeability on diffusive and electrophoretic transport is discussed in detail in [25,28].

Table 1
Physical and geometrical parameters of the model.

	Donor/receiver solution	Stratum corneum	Epidermis	Dermis
Thickness, L (μm)	1000	20	50	300
Thermal conductivity, k (W/mK)	0.6	0.2	0.209	0.293
Density, ρ (kg/m^3)	1000	1500	1110	1116
Heat capacity, c (J/kg K)	4180	3600	3600	3800
Electrical conductivity, σ (S/m)	1	$\sigma_{SC\text{-}U} = 1 \times 10^{-4}$ $\sigma_{SC\text{-}M} = 5 \times 10^{-2}$	0.1	0.15
Electrophoretic mobility, m (m^2/V s)	1.5×10^{-8}	$m_{SC\text{-}U} = 1 \times 10^{-15}$ $m_{SC\text{-}M} = 1 \times 10^{-10}$	1×10^{-9}	1×10^{-9}
Diffusion coefficient, D (m^2/s)	1.5×10^{-10}	$D_{SC\text{-}U} = 1 \times 10^{-17}$ $D_{SC\text{-}M} = 1 \times 10^{-12}$	3×10^{-11}	3×10^{-11}

3.5. Computational considerations

Axis-symmetric representations of Eqs. (1)–(9) are developed in finite volume form. The physical domain modeled is the cylindrical area that is radially centered about a single SC defect in order to capture the evolution of a single LTR. The composite representation and the region of SC surrounding the defect are depicted in Fig. 2. This cylindrical domain is represented using a curvilinear grid whose refinement is much higher within the SC. A global 1 ms time step is used during the modeled 250 ms LV pulses. After the administration of the pulses, the time step is gradually increased to 1 s. The Authors developed the computational code in the language Fortran F90. Fully implicit representations of Eqs. (1)–(4) are solved using a simple point iterative method so that convergence is established when the maximum local difference between iterations of each of the conserved variables (T, C and V) is less than 10^{-6}.

Regarding the boundary conditions, the electric potential of Eq. (3) is evaluated assuming no electrical conduction at the outer radial sides, approximating the case of a regular distribution of LTRs. During the pulse, the upper boundary is prescribed an electric potential equal to the applied voltage and the lower boundary is held constant at a zero potential value. The calcein flux at all boundaries of the system is assigned a value of zero. Initially the dimensionless solute concentration is unity in the donor solution layer and has a zero value everywhere else. The initial temperature distribution is uniform and equal to the temperature maintained in Franz diffusion cells (37 °C). To complete the computation of Eq. (1) it is assumed that the radial boundaries are thermally insulated and that at the outer axial boundaries of the solution, the temperature remains constant at the controlled solution temperature of 37 °C.

The temperature, T, the Joule heat, Q_J, and the concentration, C, are all evaluated at the cell centers while the electric potential, V, is evaluated at the cell edges. The electric potential gradient, ∇V, of the electrophoretic term in Eq. (4) is evaluated at the midpoint of the cell faces. Within the SC, the conservative equations and resistive heat of Eqs. (1)–(4) are evaluated using SC property values of the previous time step. The SC altered electrical conductivity and transport coefficients that are associated with lipid phase transitions of Eqs. (8) and (9) are updated at each time step. The specific heat of the SC lipids during phase transition are updated at each time step in using the values listed in Table 1 of Ref. [27].

4. Theoretical results and discussion

We begin our theoretical discussion with an in depth analysis of the system response to the long LV pulses. This is necessary in order to understand the physics of the transport. Here we model 3 × LV pulses of 250 ms duration that are separated by 100 ms. The computational domain is focused within the radial location near the vicinity of a pre-existing SC defect. In this case the defect has a 10 μm radius and extends from the donor solution through the SC and terminates at the viable epidermis. Note that the outer radius of the computational domain (R_O) is 250 μm and represents the small region of skin (1/400th of that of the actual experiment) that is centered around this small pre-existing defect. All other parametric inputs used for these results are given in Table 1.

4.1. General response to LV pulse

Figure 3 depicts the deposition of calcein immediately after pulse 1 (at 250 ms) in panel (a) and pulse 3 (at 950 ms) in panel (b). The perspective shown is of the axis-symmetric region centered directly about a single developing LTR. The theoretical results provide insight into the electrophoretic transport as well as the growth of the LTR.

Here, the boundary of the SC is indicated by the solid rectangular shapes on either side of the defect. The junction between the epidermis and dermis is indicated by the thick solid horizontal line at a depth of 70 μm. There are obvious indications of LTR formation that are seen in the calcein concentrations that have penetrated into the SC. Evidence of strong electrophoretic influence is seen not only in the rapid transport of solute into the skin, but also in the high concentration magnitudes within the skin.

The explanation of this high cutaneous deposition of the charged calcein lies in the influence of the electric field distribution on the electrophoretic transport. Because the electrical conductivity within the SC (even after lipid phase transition) is an order of magnitude lower than in the epidermis, the electric field experiences a sudden drop at the SC-epidermis junction [25,27,31]. Similarly the electric field in the axial 'z' direction experiences a drop at the outlet of the pre-existing pathway due to the sudden radial spreading of the field. This spreading is reflected in the shapes of the contours of Fig. 3, which spread radially outward at locations below the edges of the LTR. It is clear that there are two transport routes here: one through the pre-existing defect and one through the altered SC in the vicinity of this region: the LTR.

The localized increase in area of the SC penetrated by calcein is evidence of LTR formation. The evolution of the LTR correlates directly to the radial expansion of the calcein's penetration into the SC from pulse 1 to pulse 3. In order to better quantify parameter effects on LTR development during the pulse, the effective LTR radius, $R^+(t)$, is introduced. The effective LTR radius is defined as the minimum radial location within the SC at which the SC lipids have not experienced any thermal restructuring ($\varphi \neq 0$). Thus $R^+(t)$ is used to characterize the LTR's region of influence at any time during the applied pulse.

Figure 4 presents the transient behavior of the LTR growth and the electric current during the applied LV pulse. As implicated by the solute depositions of Fig. 3, the LTR grows radially outward during the applied pulses. Note how the increases in electric current reflect the LTR growth (Fig. 4a). As the LTR develops, the local electrical conductivity within the LTR increases, so that the electric

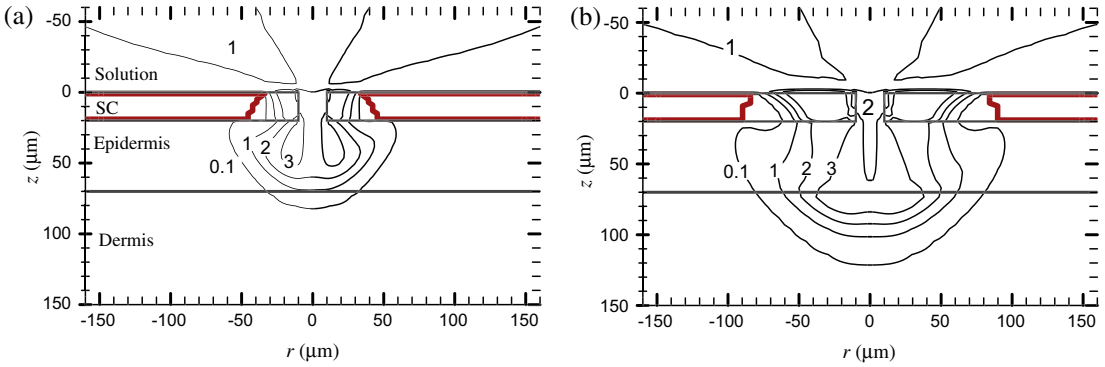

Fig. 3. Dimensionless calcein concentrations for LV pulses in the vicinity of a pre-existing defect within the SC microstructure. Times shown correspond to the end of (a) pulse 1, and the end of pulse 3 in panel (b). The solid rectangle represents the boundary of the SC, horizontal line represents the epidermal–dermal junction. Skin layers are indicated in panel (a). The bold red line corresponds to the boundary of the SC for which lipids are unaltered (for which $\varphi = 0$). (For interpretation of the references to color in this figure legend, the reader is referred to the web version of this article.)

current between electrodes increases as well. This provides a method to better interpret the electrical behavior of the experimental results. Theoretically, the increases in electric current are directly proportional to the growth of the LTR (Fig. 4a). If the transient increase of electric current during the LV pulse is representative of the LTR growth/expansion as indicated by Fig. 4a, then we can infer that the increase in the LV experimental current measurements shown in Fig. 4b, implies LTR expansion.

Recall that our computational domain has 1/400th the lateral surface area of the experiment. Thus the theoretical model (Fig. 4a) actually predicts a 0.14 A increase in current for the skin sample used in the experiment (the electric current through a single LTR needs to be multiplied by 400). Fig. 4b shows an increase in electric current of ~0.1 A which is comparable to that of the numerical model. We would like to point out that this theoretical work is intended as an exploration of the physics underlying the response of the skin to HV and LV pulses, and should not be interpreted from the perspective that the model is attempting to precisely replicate the exact experimental conditions and results. With this in mind, the discrepancy between the theoretical and experimental values of the electric current are acceptable.

In order to make direct comparisons on the quantities of solute transported into the skin, a normalized concentration ratio is used to represent the ratio of total solute transported below the SC surface to the total solute that would be contained in a layer whose outer radius is equal to that used in the experiment (5 mm). It is represented mathematically by the expression:

$$C^{+}_{SC}(t) \equiv \frac{\int_{r=0}^{R_0}\int_{z=0}^{1370\,\mu m} C(r,z,t)\,dz\,dr}{\int_{r=0}^{5000\,\mu m}\int_{z=-1000\,\mu m}^{0} C(r,z,0)\,dz\,dr} = \frac{\text{Calcein transported below the SC surface through a single LTR}}{\text{Total Calcein initially in the donor solution}} \tag{10}$$

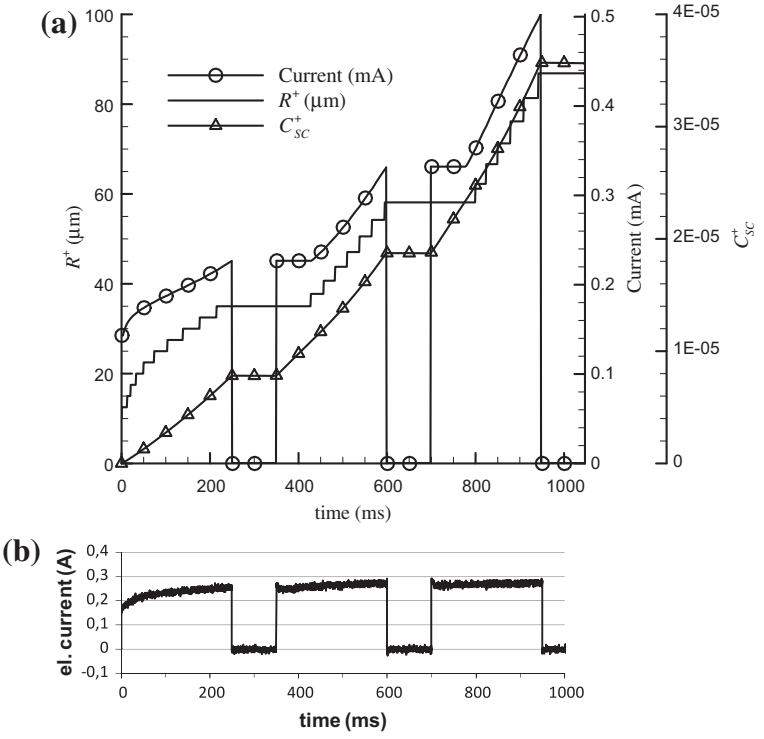

Fig. 4. (a) Theoretical predictions of model behavior during the 3 × 250 ms LV pulses. Values shown are associated with a single LTR and represent a physical domain with a lateral area that is 1/400 that of the experiment; (b) experimentally measured electric current through the entire skin sample during 3 × LV pulse protocol.

where R_O is the outer radius of the computational domain surrounding a *single* LTR and the distance from the SC surface through the skin sample and the receiver solution to the bottom electrode is 1370 μm. The total calcein that is initially stored in the donor solution corresponds to that stored in a volume of the actual experiment that is 1000 μm in depth and encompasses a radius of 5000 μm. Thus this expression can be considered as the fraction of the total calcein that is transported below the SC surface through a *single* LTR.

It is noteworthy to point out that expression (10) represents the solute delivered below the donor/SC junction and not the total solute delivered across the skin sample that was measured experimentally. Consider that by the end of the final pulse (Fig. 3b), the calcein has only been transported into the skin (at noticeable quantities) to a depth of around 150 μm, and that the receiver solution lies at a depth of 370 μm. Thus we can define the deposition of solute into the receiver solution (of thickness 1000 μm) as the total calcein transported below the dermis (at the location $z = 370$ μm). This can also be normalized by the total mass of calcein contained in a donor volume associated with the experimental set up:

$$C_R^+(t) = \frac{\int_{r=0}^{R_O}\left(\int_{z=370\ \mu m}^{1370\ \mu m} C(r,z,t)dz\right)dr}{\int_{r=0}^{5000\ \mu m}\int_{z=-1000\ \mu m}^{0} C(r,z,0)dzdr} = \frac{\text{Total Calcein transported into the receiver side}}{\text{Total Calcein initially in the donor side}} \quad (11)$$

This value, C_R^+, is a numerical representation of the relative magnitude of the transport of calcein into the receiver solution through a *single* LTR that is normalized to the total initial calcein in the donor solution. Effectively this value is the fraction of calcein that is delivered across the entire skin sample.

Eqs. (10) and (11) are numerically integrated for each control volume. They are used in this study primarily to compare the relative magnitudes of calcein delivered in a parametric analysis. The post pulsing transport due to diffusion of calcein is plotted in Fig. 5 (the results are representative of times *after* the final pulse delivered). When interpreting quantitatively the results shown in Fig. 5, keep in mind that the computed size associated with the region of transport surrounding the LTR corresponds to 1/400th of the experimental surface area associated with the experimental data of Fig. 1.

Consider that in Fig. 5, the curve representing transport into the skin – C_{SC}^+ – tells us that after the pulses are delivered, there is significant passive diffusion transport into the skin. Furthermore, the numerical model data states that at 5 h post pulse delivery, 8 times more solute has been transported through the skin than was initially deposited into the skin via LV associated electrophoresis. This implies that the experimentally measured transport of calcein (shown in Fig. 1) is not simply a reflection of the initial deposition of calcein into the skin by electrophoresis: that long after the application of the LV pulse, calcein has diffused from the donor into the receiver cell. Because this does not occur in the control or in the HV pulse scenarios, we can conclude that the LV pulse results in an alteration of the SC barrier properties that allow for extended diffusion transport: this is consistent with the increase in permeability associated with the presence of LTRs.

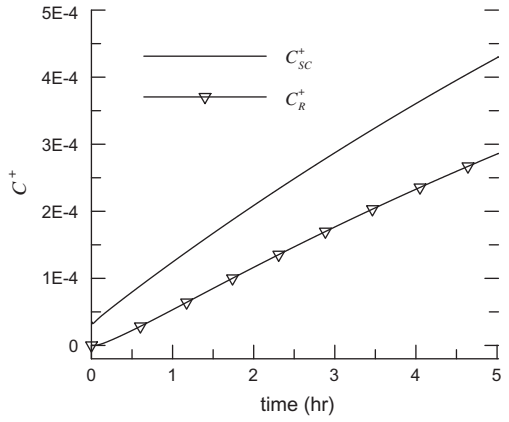

Fig. 5. Post pulse diffusion of solute into the skin, just below the SC (C_{SC}^+), and through the skin into the receiver solution (C_R^+).

4.2. Explanation of experimental phenomena

The principal motivation of this work is to try to reconcile the experimental results with the generally accepted belief that more pulses equal greater transport. In order to better understand the experimental phenomena observed when HV and LV type pulses are used in combination, we look again to the effects when the pulses are applied separately. The HV pulses alone result in an increase in electrical conductivity, as measured during pulse delivery (data not shown, see [22] for details), but negligible increases in permeability of calcein transport: this implies the expected cell-size pathways through the SC which are large enough for electric current, but too small for significant diffusion of calcein. The LV pulses alone result in gradual increases in electrical conductivity and result in long term increases in diffusion related transport of calcein: this is in line with the creation of the LTR during the LV pulse. We infer from this then that the cell-size pathways within the SC resulting from the HV pulse somehow inhibit the formation of the LTR which result from the LV pulse. In the following discussion, the influences of (i) the size and (ii) the distribution number of these HV-initiated electropores on subsequent LTR development during the LV are considered.

The pre-existing region, whose thermo-electrical properties are modeled to be the same as the donor solution, is used to approximate a cluster of cell-size pathway produced by the HV pulse. The effect of pre-existing pathway size, R_P, has a strong influence on total solute transported during and after the LV pulse. This is because the size strongly influences the electric field distribution that is evaluated from Eq. (3) which in turn is seen in the Joule heat of Eq. (2) and the temperature rises of Eq. (1). As the local temperature rises above lipid phase transition temperatures, and heat is added to the SC lipids, the LTR begins to grow. This is seen in Fig. 6a where the LTR growth is strongly dependent on the pre-existing pathway size. In fact is appears that there exists a lower limit of pre-existing pathway size for which substantial LTR growth can be initiated. Consider the results of the small diameters: $R_P = 5$ μm and $R_P = 2.5$ μm cases for which the LTRs grow very slowly. In the smallest case, it seems that the cell-size pathway does not develop further over the duration of the applied pulse. This seems to imply that the smaller pathways require much longer pulses in order to generate sufficient Joule heating for lipid melting. The theoretical implications of Fig. 6a are that if the pathways are not clustered together in localized regions of sufficient effective diameter (as is expected for an HV pulse), the LV pulse requires a much longer pulse duration in order to deliver sufficient power to induce lipid phase transition.

Next consider the density of the pre-existing pathways. We anticipate that an HV pulse increases the density distribution. This can be represented by a lowered value of R_O in the computational domain. Fig. 6b shows that the LTR evolution during the LV pulse is strongly affected by the outer computational domain radius. In fact it suggests that for a given skin sample, there is some minimum value of R_O below which LTR evolution does not take place in the observed time during the 3×250 ms LV pulses. That there are pathway densities beyond which LTR evolution does not occur

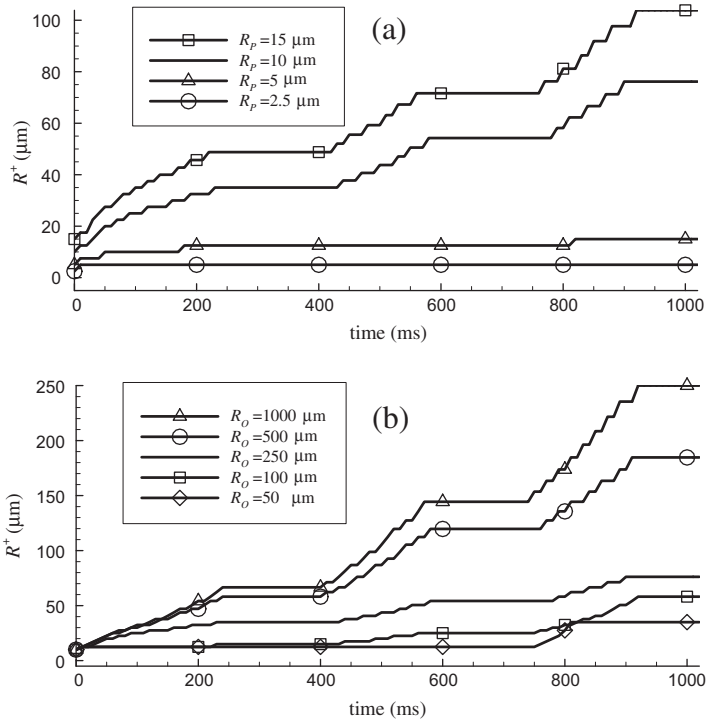

Fig. 6. (a) Influence of pre-existing pathway size on the LTR evolution during LV pulses. The outer computational domain radius, R_O is 250 μm; (b) influence of pathway density on the LTR evolution. Pathway density is inversely proportional to the square of the outer domain radius, R_O^2. The pre-existing pathway radius R_P = 10 μm.

during the LV pulse is in alignment with our interpretation of the experimental results of Fig. 1 which imply that in some instances when the HV pulses precede the LV pulses, the LV pulses result in negligible transport.

The physical explanation of this phenomenon again lies in the consideration of the electric current density. Note that the LTR is initiated and grows as a consequence of SC lipid thermal alterations which result from localized resistive heating during the LV pulse. In order for this resistive heating to provide sufficient thermal energy to initiate these lipid thermal phase transitions, a high current density in the small pre-existing region of higher electrical conductivity encompassed by R_P is required. For a low amplitude LV pulse, such a high current density can only occur when within the SC there exist only a few regions of high permeability to electric current. When the pathway density is increased, for a given global domain, the global distribution of electric current is distributed among more pre-existing pathways. This is likely to result in a lower electric current within each pathway (and thus less heating). The calculations used to arrive at Fig. 6b represent higher pathway densities with smaller computational domain sizes: so that there is less total current available for a smaller R_O (representing a higher density distribution of pathways, associated with HV pulses).

Therefore, the reason for the negative effect of the preceding HV pulses may be precisely the large number of small cell-level pathways created with the HV pulses. As the electric current during the following LV pulses flows predominantly through these low-resistance pathways, the current density and consequently the thermal expansion of these pathways is lower, resulting in a lower transdermal molecular transport.

5. Conclusions

We have considered the general view held in the field: that more electroporation pulses automatically equate to higher total solute transport and have shown that this view must be carefully considered. The experimental results show that under certain conditions, preceding the low voltage pulse by a short high intensity pulse results in less transport than the LV pulse alone. We have conducted a series of theoretical investigations that show that the increase in permeability to transport resulting from the large LTR evolution is hindered when the pre-existing (to the LV pulse) SC has a high density of very small defects. Such defect size and distribution are attributed to the high intensity HV pulse. Our theoretical study, which is based on the conservation of current, the conservation of energy, and the empirically observed lipid thermal behavior, shows that the conditions associated with the HV prepulsing result in the requirement of much longer times in order to sustain LTR evolution. Having determined that the LTR evolution is highly dependent on SC condition, future work of this group is concerned with using this information in order to maximize the potential for LTR development while minimizing the risk of thermal damage to the viable tissue layers beneath the SC.

Acknowledgments

Research was performed in the scope of LEA EBAM and was in part financed by the European Regional Development Fund (Biomedical Engineering Competence Center, Slovenia), the Slovenian Research Agency (P2-0249), and the New Zealand Royal Society's Marsden Fund. A great part of this work was carried out during the Short Term Scientific Mission (Applicant: Barbara Zorec, Reference Number COST-STSM-TD1104-14357) funded by COST TD1104 (www.electroporation.net).

References

[1] B. Zorec, V. Préat, D. Miklavčič, N. Pavšelj, Active enhancement methods for intra- and transdermal drug delivery: a review, Slovenian Med. J. 82 (2013).
[2] T. Blagus, B. Markelc, M. Cemazar, T. Kosjek, V. Preat, D. Miklavcic, et al., In vivo real-time monitoring system of electroporation mediated control of transdermal and topical drug delivery, J. Controlled Release 172 (2013) 862–871.

[3] R. Vanbever, U.F. Pliquett, V. Préat, J.C. Weaver, Comparison of the effects of short, high-voltage and long, medium-voltage pulses on skin electrical and transport properties, J. Controlled Release 60 (1999) 35–47.
[4] Pliquett, Mechanistic studies of molecular transdermal transport due to skin electroporation, Adv. Drug Deliv. Rev. 35 (1999) 41–60.
[5] Weaver, Vaughan, Chizmadzhev, Theory of electrical creation of aqueous pathways across skin transport barriers, Adv. Drug Deliv. Rev. 35 (1999) 21–39.
[6] U. Pliquett, C. Gusbeth, Surface area involved in transdermal transport of charged species due to skin electroporation, Bioelectrochemistry 65 (2004) 27–32.
[7] U.F. Pliquett, R. Vanbever, V. Preat, J.C. Weaver, Local transport regions (LTRs) in human stratum corneum due to long and short 'high voltage' pulses, Bioelectrochem. Bioenerg. 47 (1998) 151–161.
[8] A.-R. Denet, R. Vanbever, V. Préat, Skin electroporation for transdermal and topical delivery, Adv. Drug Deliv. Rev. 56 (2004) 659–674.
[9] U. Pliquett, C. Gusbeth, R. Nuccitelli, A propagating heat wave model of skin electroporation, J. Theor. Biol. 251 (2008) 195–201.
[10] U. Pliquett, S. Gallo, S.W. Hui, C. Gusbeth, E. Neumann, Local and transient structural changes in stratum corneum at high electric fields: contribution of Joule heating, Bioelectrochemistry 67 (2005) 37–46.
[11] U.F. Pliquett, T.E. Zewert, T. Chen, R. Langer, J.C. Weaver, Imaging of fluorescent molecule and small ion transport through human stratum corneum during high voltage pulsing: localized transport regions are involved, Biophys. Chem. 58 (1996) 185–204.
[12] F.M. André, J. Gehl, G. Sersa, V. Préat, P. Hojman, J. Eriksen, et al., Efficiency of high- and low-voltage pulse combinations for gene electrotransfer in muscle, liver, tumor, and skin, Hum. Gene Ther. 19 (2008) 1261–1271.
[13] N. Pavselj, D. Miklavcic, A numerical model of permeabilized skin with local transport regions, IEEE Trans. Biomed. Eng. 55 (2008) 1927–1930.
[14] N. Pavšelj, D. Miklavčič, Resistive heating and electropermeabilization of skin tissue during in vivo electroporation: a coupled nonlinear finite element model, Int. J. Heat Mass Transfer 54 (2011) 2294–2302.
[15] N. Pavšelj, D. Miklavčič, Numerical modeling in electroporation-based biomedical applications, Radiol. Oncol. 42 (2008) 159–168.
[16] D.P. Tieleman, The molecular basis of electroporation, BMC Biochem. 5 (2004) 10.
[17] P. Kramar, L. Delemotte, A. Macek Lebar, M. Kotulska, M. Tarek, D. Miklavcic, Molecular-level characterization of lipid membrane electroporation using linearly rising current, J. Membr. Biol. (2012) (n.d.) 651–659.
[18] U.F. Pliquett, C.A. Gusbeth, Perturbation of human skin due to application of high voltage, Bioelectrochemistry 51 (2000) 41–51.
[19] U. Pliquett, R. Langer, J.C. Weaver, Changes in the passive electrical properties of human stratum corneum due to electroporation, Biochim. Biophys. Acta 1239 (1995) 111–121.
[20] M.R. Prausnitz, Do high-voltage pulses cause changes in skin structure?, J Controlled Release 40 (1996) 321–326.
[21] R. Vanbever, V. Préat, In vivo efficacy and safety of skin electroporation, Adv. Drug Deliv. Rev. (1999) (n.d.) 77–88.
[22] B. Zorec, S. Becker, M. Reberšek, D. Miklavčič, N. Pavšelj, Skin electroporation for transdermal drug delivery: the influence of the order of different square wave electric pulses, Int. J. Pharm. (2013).
[23] V. Regnier, N. De Morre, A. Jadoul, V. Préat, Mechanisms of a phosphorothioate oligonucleotide delivery by skin electroporation, Int. J. Pharm. 184 (1999) 147–156.
[24] S. Satkauskas, F. André, M.F. Bureau, D. Scherman, D. Miklavcic, L.M. Mir, Electrophoretic component of electric pulses determines the efficacy of in vivo DNA electrotransfer, Hum. Gene Ther. 16 (2005) 1194–1201.
[25] S. Becker, Transport modeling of skin electroporation and the thermal behavior of the stratum corneum, Int. J. Therm. Sci. 54 (2012) 48–61.
[26] S.M. Becker, A.V. Kuznetsov, Local temperature rises influence in vivo electroporation pore development: a numerical stratum corneum lipid phase transition model, J. Biomech. Eng. 129 (2007) 712–721.
[27] S.M. Becker, A.V. Kuznetsov, Thermal in vivo skin electroporation pore development and charged macromolecule transdermal delivery: a numerical study of the influence of chemically enhanced lower lipid phase transition temperatures, Int. J. Heat Mass Transfer (2008) 2060–2074.
[28] P.A. Cornwell, B.W. Barry, J.A. Bouwstra, G.S. Gooris, Modes of action of terpene penetration enhancers in human skin; differential scanning calorimetry, small-angle X-ray diffraction and enhancer uptake studies, Int. J. Pharm. 127 (1996) 9–26.
[29] U. Jacobi, M. Kaiser, R. Toll, S. Mangelsdorf, H. Audring, N. Otberg, et al., Porcine ear skin: an in vitro model for human skin, Skin Res. Technol. 13 (2007) 19–24.
[30] D. Miklavčič, N. Pavšelj, F.X. Hart, Electric properties of tissues, in: Wiley Encyclopedia of Biomedical Engineering, John Wiley & Sons Inc., 2006.
[31] S.M. Becker, Skin electroporation with passive transdermal transport theory: a review and a suggestion for future numerical model development, J. Heat Transfer 133 (2011) 011011.
[32] R.J.H. Stenekes, A.E. Loebis, C.M. Fernandes, D.J.A. Crommelin, W.E. Hennink, Controlled release of liposomes from biodegradable dextran microspheres: a novel delivery concept, Pharm. Res. 17 (2000) 664–669.
[33] J. Zhao, Sol–Gel Immobilized Liposomes as an Artificial-Cell-Based Biosensor for Listeriolysin O Detection, Doctoral Dissertation, Purdue University, 2008.
[34] D. Milanova, R.D. Chambers, S.S. Bahga, J.G. Santiago, Electrophoretic mobility measurements of fluorescent dyes using on-chip capillary electrophoresis, Electrophoresis 32 (2011) 3286–3294.
[35] Y. Guy, Determination and Implications of Physicochemical Properties of the Brain (2011).
[36] Z. Zador, M. Magzoub, S. Jin, G.T. Manley, M.C. Papadopoulos, A.S. Verkman, Microfiberoptic fluorescence photobleaching reveals size-dependent macromolecule diffusion in extracellular space deep in brain, FASEB J. 22 (2008) 870–879.